

Multiple microdischarge dynamics in dielectric barrier discharges

Xudong "Peter" Xu^{a)} and Mark J. Kushner^{b)}

University of Illinois, Department of Electrical and Computer Engineering, 1406 West Green Street, Urbana, Illinois 61801

(Received 21 May 1998; accepted for publication 21 July 1998)

Dielectric barrier discharges (DBDs) are pulsed atmospheric pressure devices in which the plasma forms as an array of microdischarges having diameters expanding from 10 to 100's μm and area densities of 10 to 100's cm^{-2} . The microdischarges are < 10 's ns in duration and are terminated by charging of the dielectric barrier which removes voltage from the gap. If microdischarges are spaced sufficiently close together they may interact during their expansion. In this article, we discuss results from a two-dimensional plasma hydrodynamics model for microdischarge development in DBDs with the goal of investigating the interaction between closely spaced microdischarges. We find that the efficiency of ionization is only moderately affected by microdischarges which expand into physical contact. The residual charge left on the dielectric following a current pulse can, however, significantly impact the spatial extent of the subsequent microdischarges. During expansion the underlying dielectric charges to progressively larger radii as the microdischarge expands. This leads to voltage collapse in the center of the microdischarge prior to the outer radius. In attaching gas mixtures larger rates of attachment relative to ionization at the lower values of the electric field/number density produce cores which are highly electronegative, surrounded by shells of higher electron density. © 1998 American Institute of Physics. [S0021-8979(98)07620-8]

I. INTRODUCTION

Dielectric barrier discharges (DBDs), or silent electrical discharges, are being developed for plasma remediation of toxic gases and as advanced ultraviolet lighting sources.¹⁻¹⁰ The plasma in DBDs is sustained between parallel electrodes of which one (or both) is covered by a dielectric. The plasma operates in a pulsed filamentary mode and is composed of microdischarges having diameters of 10–100's μm , durations of 10's ns and area densities of 10–100's cm^{-2} . An alternating voltage of a 3–15 kV is applied at repetition rates of 100's Hz–10's kHz across the 2–4 mm gap. When a microdischarge is initiated in a DBD, the underlying dielectric is electrically charged, thereby removing voltage from the gap. The microdischarge is terminated when the gap voltage falls below the self-sustaining value, thereby preventing arcing. If, on the following half cycle, a microdischarge occurs at the same location, the voltage across the gap can, in fact, be larger than the applied potential since the previously charged dielectric now adds to the applied voltage.

The propagation of streamers across gaps has been investigated by a number of workers, in particular Morrow and Lowke¹¹ and Dhali and Williams.¹² The development of microdischarges in the context of DBDs has been previously computationally investigated by Braun *et al.*¹³ They developed a two-dimensional (2D) model (r, z) for a single streamer to study the breakdown process following streamer propagation between the electrodes and its subsequent radial expansion in air. Continuity equations for charged species and O atoms were solved in conjunction with Poisson's

equation. Charge accumulation on the dielectric was also tracked. They found that the streamer expands from a few microns to 200–300 μm during 30–40 ns current pulses. With a discharge gap of 1 mm and dielectric thickness of 3 mm having $\epsilon/\epsilon_0=5$ (1.5 pF/cm²), peak electron and oxygen atom densities of $1 \times 10^{14} \text{ cm}^{-3}$ and $1 \times 10^{17} \text{ cm}^{-3}$, respectively, were predicted. The temperature rise in the positive column portion of the discharge was only 6–7 K, while in the cathode layer the temperature rise was 150–200 K. For $\epsilon/\epsilon_0=50$, the temperature rises were 25 and 800 K. For those temperature rises, hydrodynamic effects can be expected to be important. Eliasson and Kogelschatz¹⁴ developed a similar two-dimensional (r, z) model to study streamer dynamics in Xe and O₂. They found that streamer expansion and dielectric charging occurred on time scales of 30–50 ns to radii of 250–300 μm . They also found that the charge collected on the dielectric generally increases with dielectric capacitance, implying thin dielectrics with large ϵ result in large energy deposition in the gas.

These previous modeling studies addressed radially symmetric microdischarge dynamics at moderate to low energy deposition. In this article, we report on results from a modeling study in which the complementary problem of the expansion of multiple, and hence radially asymmetric, microdischarges in close vicinity is investigated. The final application of interest is plasma remediation of toxins from air, and so we have investigated N₂ and dry air (N₂/O₂) discharges as examples of nonattaching and attaching discharges. The model we used in this study is described in Sec. II. Parametric studies for microdischarge development for 1–4 adjacent microdischarges will be discussed in Sec. III. Our concluding remarks are in Sec. IV.

^{a)}Electronic mail: xxu@uiuc.edu

^{b)}Electronic mail: mjk@uiuc.edu

II. DESCRIPTION OF THE MODEL

The 2D model of DBDs used in this study is the analog of the one-dimensional (1D) model described in Ref. 15. With the exception of those specific items discussed below, the physical model, equations solved and mathematical techniques used in the 2D model are the same as in the 1D model. Since the physical model and equations are discussed in detail in Ref. 15, we will only briefly review them here.

The flow of the 2D model is as follows. We resolve the two-dimensions parallel to the electrodes and therefore do not address the cathode fall dynamics. This model is, then, addressing positive column characteristics of the microdischarge. To begin, we select a gas mixture, gap spacing, dielectric properties and voltage pulse shape. A small initial electron density (10^8 – 10^9 cm^{-3}) having a small radial extent (a few microns) is specified as an initial condition. The voltage pulse is applied and the compressible Navier–Stokes equations are solved for continuity, momentum conservation, and energy density of the gas mixture. Continuity equations are solved for all heavy particle species (neutrals and ions) and electrons.

The transport equations were explicitly integrated in time using a fourth order Runge–Kutta–Gill technique. Spatial derivatives are formulated using conservative finite difference donor cell techniques on a staggered mesh where mass density and temperature are solved for at cell vertices, whereas momentum is obtained at cell boundaries. The 2D mesh was rectilinear with (usually) equal spacing in each direction. In the cases where we have bulk gas flow through the device (e.g., a “right to left” flow field), we simply superimposed a bulk flow velocity \mathbf{v}_b parallel to the electrodes. To account for no-slip flow and formation of boundary layers in the axial direction, we include an axial shear term in the viscous drag term of the momentum equation. This term is formulated using $\Lambda = d/\pi$ (d is the gap spacing) as the transport length.

In this work, we are not solving Poisson’s equation for the electric potential. The axial electrical field in provided by solving circuit equations for the pulse power apparatus and dielectric charging in the manner described in Ref. 15. Given the E/N (electric field/number density) in the plasma, electron impact rate coefficients are obtained using the local field approximation from a two-term spherical harmonic expansion of Boltzmann’s equation for the electron energy distribution. In practice, Boltzmann’s equation is solved off line for a range of values for E/N and a look-up table of rate coefficients and electron transport coefficients is constructed. This table is then interpolated during execution of the model.

In the plasma chemistry model, the densities for all species, the gas temperature and the charge density on the dielectric are updated independently at each mesh point while excluding transport. The method allows us to use a different integration time step at each mesh point, which tends to be short ($<10^{-11}$ s) in the active microdischarge region and longer outside the microdischarge. After the update of the local kinetics, the densities are then updated based on transport in hydrodynamic model where the momentum and energy equations are also simultaneously solved. We enforced

electrical neutrality and so the electron density at each mesh point is forced to be equal to the charge weighted sum of the ion densities.

Initial conditions are generated by specifying (or randomly distributing) a center point for each microdischarge in the 2D domain. The microdischarge is assumed to be initially radially symmetric and composed of a seed electron density having a super-Gaussian profile with peak density of $n_0 = 10^9$ cm^{-3} and radius $r_0 = 15$ μm . Initial electron densities which would be smaller than $10^{-4}n_0$ are set equal to zero. The pressure is one atmosphere at 400 K. One electrode is covered by 0.5 mm thickness of a dielectric having a permittivity of $25\epsilon_0$ with 0.25 cm gas gap. The applied voltage is a square pulse of specified duration and magnitude.

III. MULTIPLE MICRODISCHARGES

The dynamics of a single microdischarge were discussed in Ref. 15. In summary, we found that as the microdischarge expands and charges the dielectric, voltage across the gap first collapses at the center of the microdischarge. This produces a corresponding drop in the E/N in the bulk plasma and a commensurate decrease in the rates for high threshold collisions such as electron impact ionization. There is a corresponding increase in low threshold processes, such as electron-ion recombination in particular. In electron attaching gas mixtures, this collapse of voltage often also results in an increase in the attachment rate in the center of the microdischarge. Meanwhile, at the periphery of the microdischarge, the plasma diffuses into regions where the dielectric is uncharged and the entire voltage is still across the gap. Avalanche occurs at those locations which then advances the microdischarge. The end result is that electron avalanche is limited to an expanding shell. The center of the microdischarge typically has a lower electron density, a different ion composition than the expanding shell and often has a large negative ion density.

We also found that in many cases the dielectric under the microdischarge charges to essentially the line voltage. When the applied voltage is pulled to zero at the end of a square wave voltage pulse, the charged dielectric provides a “negative” voltage across the gas gap whose value is almost equal to the pulse line voltage. The microdischarge experiences a second rapid avalanche since the microdischarge region consists of “preionized” plasma which has not fully recombined. Plasma properties for a single microdischarge obtained with the 2D model are essentially the same as those obtained with the 1D model provided that a minimum resolution is maintained (≈ 2 μm) to prevent the microdischarge from being distorted due to edge effects.

The electron density is shown in Fig. 1 for two microdischarges in N_2 separated by 300 μm for a square wave 40 ns voltage pulse of 12 kV. Results are shown for times of 0.8, 26, 41, and 100 ns. 1D slices of the electron density through the axis of symmetry are shown in Fig. 2. Only the upper half of the microdischarges is shown in Fig. 1, taking advantage of symmetry across the lower horizontal axis. As in Ref. 15, We have chosen conditions for which the micro-

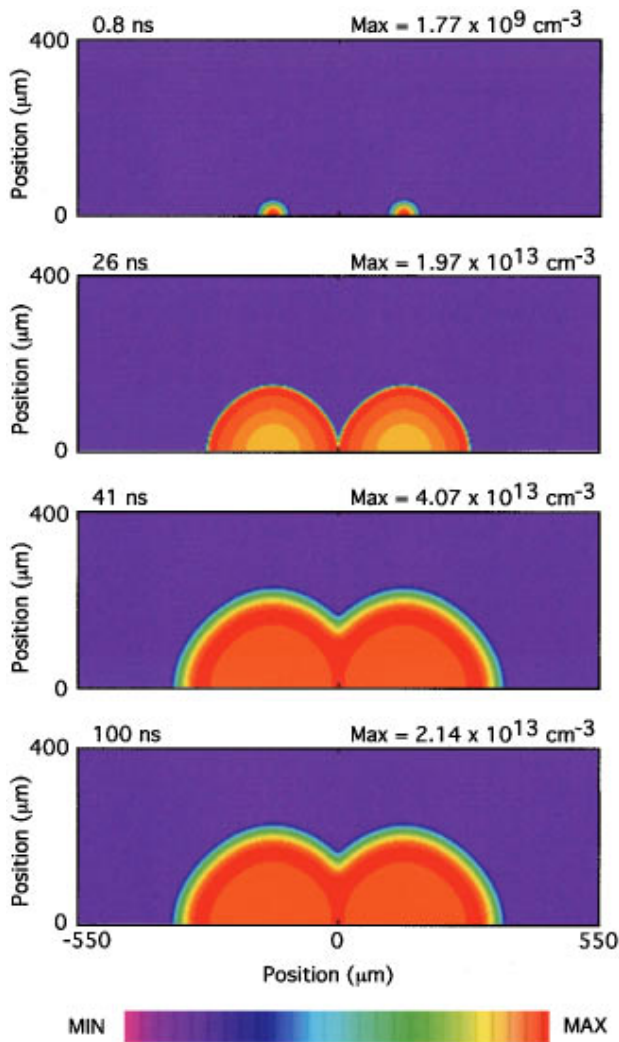


FIG. 1. Electron density for two closely spaced microdischarges in N_2 at 0.8, 26, 41 and 100 ns. The separation of the two microdischarges is 300 μm and the applied voltage is a 40 ns square wave pulse at 12 kV. The maximum electron density in each frame is indicated. The color scale is linear with density. The results are symmetric across the bottom axis.

discharge will continue to expand for the duration of the voltage pulse in order to reduce the importance of issues related to surface conductivity of the substrate. The expanding microdischarges retain their initial circular profiles until they collide. Note the somewhat hollow appearance of the microdischarges. As in the case of the single microdischarge, charging of the dielectric in the center of the microdischarges produces a collapse of the E/N in the bulk plasma which reduces the rate of electron generating collisions (e.g., ionization) and increases the rate of electron consuming collisions, in this case dissociative recombination. At 40 ns, when the voltage is pulled to zero, the electric field resulting from charging of the dielectric produces a secondary discharge in a similar manner as for the single discharge. Further expansion does not occur during the secondary avalanche since the dielectric outside the microdischarge is not charged.

When the microdischarges collide, a peak in the electron density occurs at the interface, having an enhancement of $\approx 13\%$ over the single microdischarge. This increase can be attributed to two causes. The first, in a sense, is a conse-

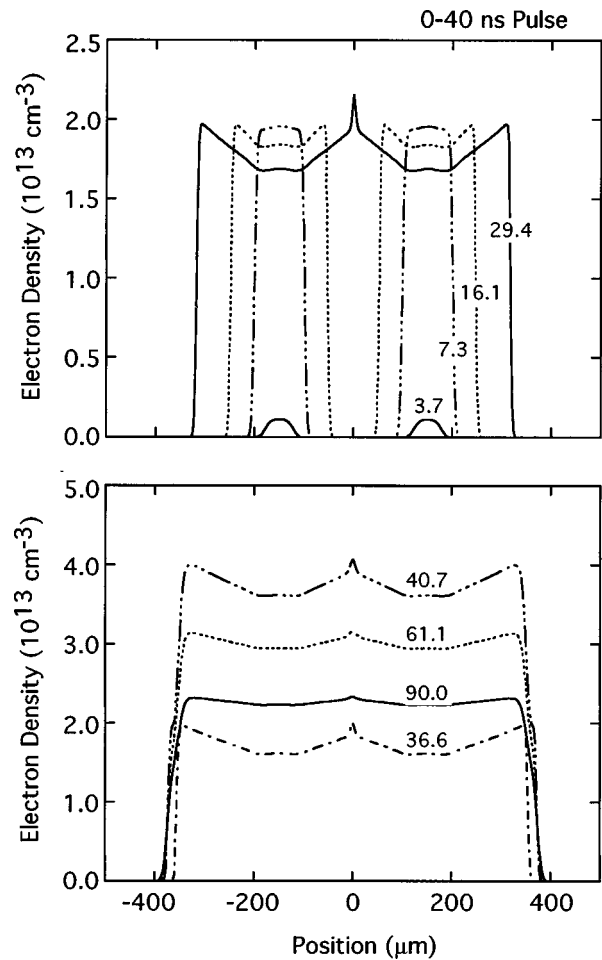


FIG. 2. Electron density along the axis of symmetry at various times in an N_2 microdischarge for the conditions of Fig. 1. The curves are labeled with their time (ns) after the start of the voltage pulse. The peak electron density occurs at the interface of the expanding microdischarges with a 13% increase compared to a single microdischarge.

quence of the initial conditions. Electrons from the microdischarge diffuse into regions of uncharged dielectric, followed by avalanche which begins charging the dielectric. The peak electron density occurs as the voltage across the gap falls below the self-sustaining value and the net electron generation turns negative. The peak electron density therefore weakly depends on the initial electron density since there is some dynamic “overshoot” of the equilibrium conditions. Since we have contributions from expansion by both microdischarges to the effective n_0 at the interface, the initial electron density for avalanche at that location is larger. As a consequence, the maximum electron density is larger. The second effect is hydrodynamic in nature. The ions and neutrals can, from a hydrodynamic standpoint, be considered well coupled fluids. The inertia of the expanding plasma column results in the shells of the colliding microdischarges producing a higher gas density. Since the ions are entrained in this flow, the ion density increases commensurably.

The plasma expansion of the microdischarges terminates on the sides where the collision occurs, but continues to expand on the opposite sides. The end result is an elongated appearance to the microdischarges. The microdischarges do not “pass through” each other as would, for example, ex-

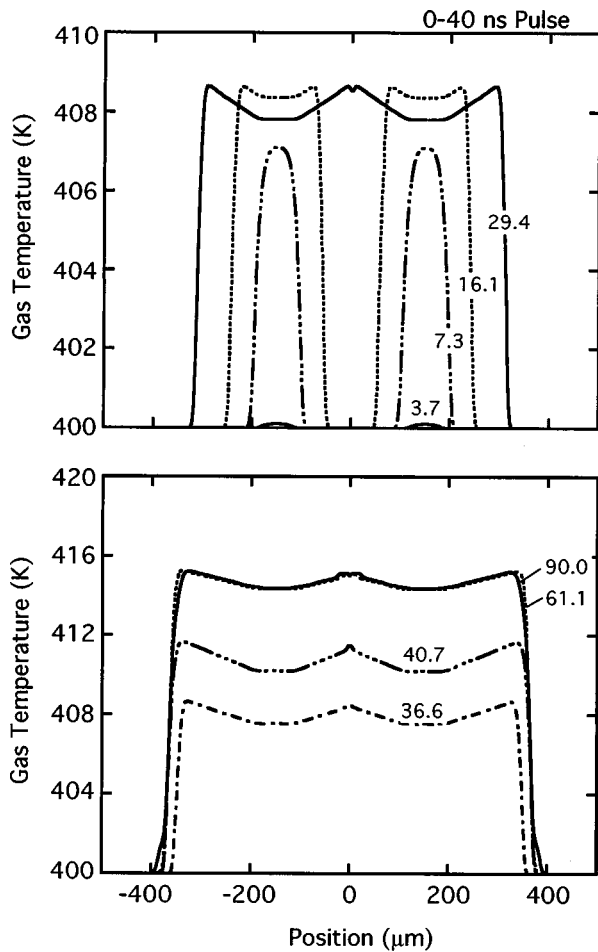


FIG. 3. Gas temperature along the axis of symmetry at various times in an N_2 microdischarge for the conditions of Fig. 1. The curves are labeled with their time (ns) after the start of the voltage pulse. Unlike the electron density, the gas temperature continues to increase after the voltage pulse is terminated due to dissipation of energy from excited states of N_2 into translational modes.

panding acoustic waves. Recall that the expansion of the microdischarges is sustained by diffusion of electrons into regions in which the dielectric is uncharged, thereby enabling avalanche and growth of the microdischarge. Since at the interface, electron diffusion occurs into regions in which the dielectric is already charged, further avalanche and expansion do not occur.

The gas temperature in the microdischarge depends on the total energy deposition, manner of dissipation of deposited energy and change in enthalpy due to chemical reactions and radiative decay of excited states. Gradients in temperature also produce pressure gradients which can lead to advection. For example, 1D slices of the gas temperature and total gas mass density are shown in Figs. 3 and 4 for the two microdischarges in N_2 . During and just after the voltage pulse the gas temperature increases by only 8 K and has profiles similar to the electron distribution with the exception that there is a short delay in time resulting from collisional deexcitation of excited states. After 74 ns, the gas temperature in the microdischarge continuously increases with time as excited states of N_2 are quenched and dissipate their energy into translation modes. There is an additional temperature rise of ≈ 7 K from 0.1 to 0.37 μ s producing a total

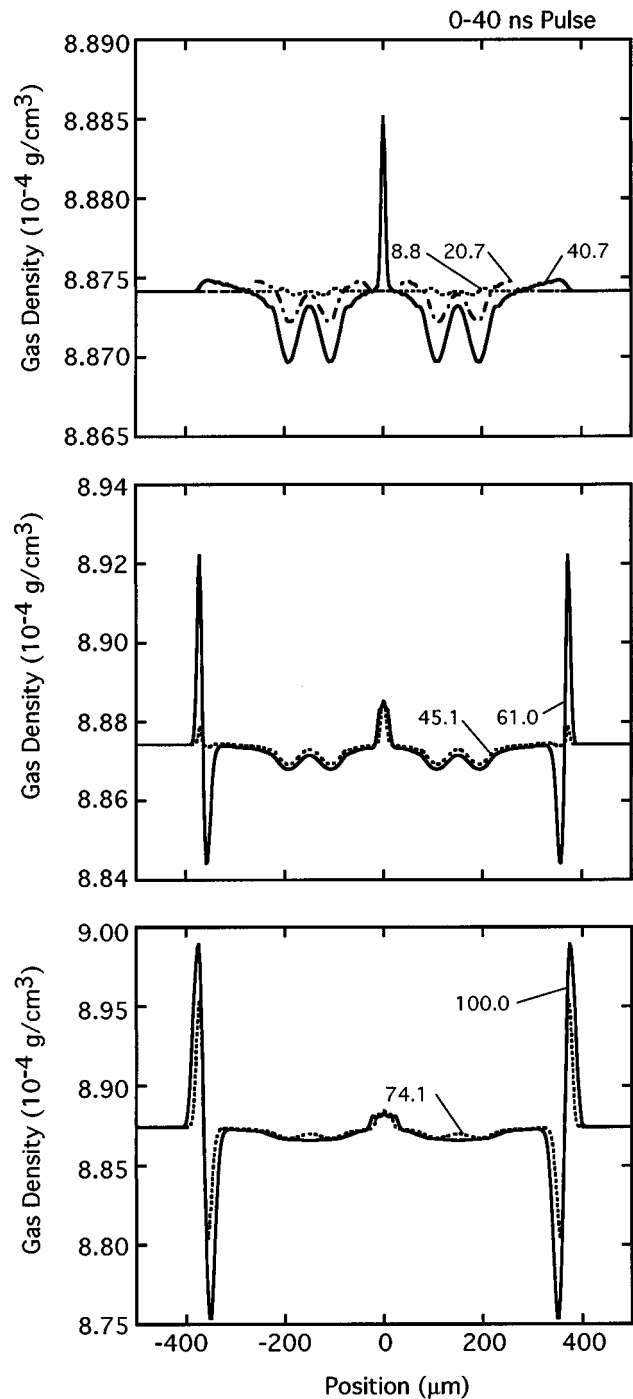


FIG. 4. Gas density along the axis of symmetry at various times for the conditions of Fig. 1. The curves are labeled with their time (ns) after the start of the voltage pulse. At long times, the gas density profiles resemble a weak blast wave.

temperature rise of about 24 K. The resulting gas density, shown in Fig. 4, shows a corresponding rarefaction and compression which resembles a weak "blast wave." The gas densities do not directly correlate to the inverse of the gas temperature due to inertial effects during the short pulse. To first order, the energy deposition appears to occur instantaneously, followed by acceleration by the resulting pressure gradient. The gas density is marginally rarefied in the center of the microdischarge during the current pulse and compressed at the interface and edges. Significant rarefaction and

compression only occur after termination of the pulse. As time proceeds, and the advective expansion slowly continues, the minimum and maximum mass densities can be found near the edge of the avalanche region.

Given the random location of microdischarges, it is conceivable that a cluster of discharges might occur in proximity of each other. To investigate this possibility, four closely spaced microdischarges were simulated using the standard conditions with the exception that the line voltage is 11 kV. The electron density during and following the 40 ns voltage pulse is shown in Fig. 5 at 0.8, 14, 41, and 100 ns. The expanding microdischarges retain their initial circular shapes until they collide. At $t=14$ ns the two closest microdischarges contact one another, thereby stalling their expansion along the interface. The other microdischarges continue to expand until they too collide with their neighbors. Their expansion then stalls and they coalesce. Note that the expanding shell of high electron density is ultimately located at the periphery of the coalesced microdischarges.

The microdischarge dynamics in dry air ($N_2/O_2=80/20$) differ from those in pure nitrogen. Since O_2 has a larger ionization rate than N_2 for a given E/N , a microdischarge in dry air at high E/N produces a larger electron density and has a higher rate of expansion. At low E/N , however, electron attachment ($O_2 + e \rightarrow O + O^-$ and $O_2 + e + M \rightarrow O_2^- + M$) adds to dissociative recombination to more rapidly decrease the electron density compared to N_2 . For example, 1D slices of electron densities through dry air microdischarges are shown in Fig. 6 for a line voltage of 12 kV. The two microdischarges are separated by 0.3 mm. Due to the addition of the attachment processes, the electron density in the interior of the microdischarge decreases more rapidly after the dielectric charges and E/N collapses compared to the N_2 microdischarges. As a result, the spike in electron density where the microdischarges collide is more pronounced, being 50% higher than in pure N_2 .

For lower applied voltages, the smaller electron density in the core of the microdischarges for $N_2/O_2=80/20$ gas mixtures reduces the current density to a sufficiently low value that the dielectric cannot fully charge. As a consequence, there is residual E/N across the core of the microdischarge for the full duration of the voltage pulse. For example, electron densities and voltage across the gap are shown in Fig. 7 for dry air microdischarges with a line voltage of 8.5 kV. Since in this gas mixture the attachment rate peaks at a nonzero E/N , the residual, but sub-avalanche, electric field in the middle of the microdischarges actually produces more net electron loss by attachment. The end result is more hollow-looking shells for the microdischarges and a more pronounced peaking of the electron density in the overlap region. Due to the incomplete charging of the dielectric, when the voltage is pulled to zero at the end of the pulse, the electric field produced by the charge is also sub-avalanche in its strength, and serves only to increase the rate of attachment. As a consequence, the microdischarges are rapidly quenched compared to those for N_2 .

The different spatial dependencies and ion compositions of the N_2/O_2 microdischarges when the dielectric is fully charged and not fully charged are shown in Fig. 8. Here we

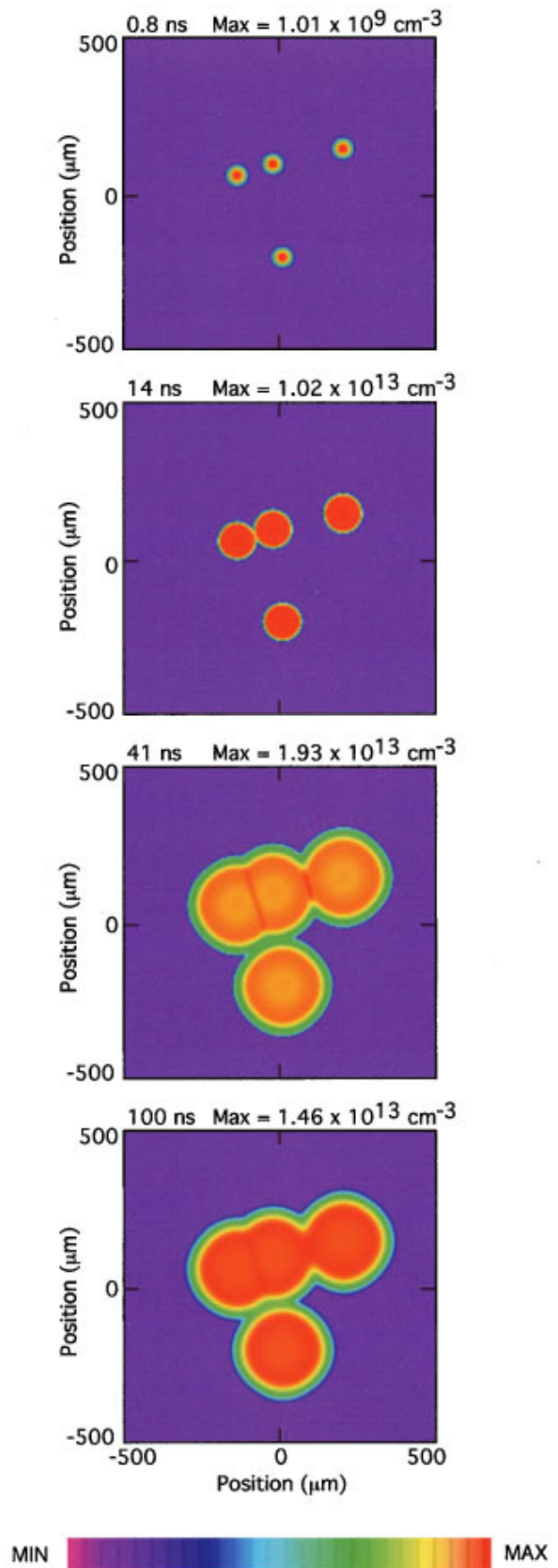


FIG. 5. Electron density for four closely spaced microdischarges in N_2 at 0.8, 14, 41, and 100 ns. The applied voltage is a square wave 40 ns pulse at 11 kV. The color scale is linear with density.

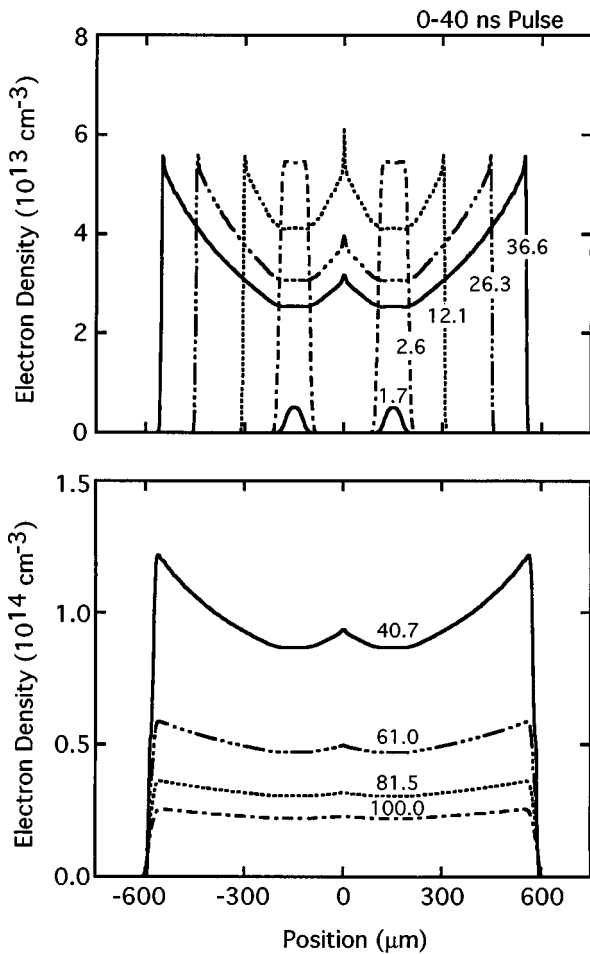


FIG. 6. Electron density along the axis of symmetry in an $N_2/O_2=80/20$ microdischarge. The curves are labeled with their time (ns) after the start of the voltage pulse. The separation of the two microdischarges is $300 \mu m$ and the applied voltage is a square wave 40 ns pulse at 12 kV. The larger rate of electron loss at low E/N in the center of the microdischarge produces a more hollow appearing electron density.

show the ion and electron densities for $N_2/O_2=80/20$ microdischarges at 36 ns for line voltages of 8.5 and 12 kV. The separation between the microdischarges is $200 \mu m$ in order to insure that they will collide during the 40 ns voltage pulse. For the lower voltage case, the current density is low enough that the dielectric is not fully charged, leaving an electric field in the center of the microdischarges which is sub avalanche and promotes attachment. The charged particle composition is dominantly negative ions and positive ions in the middle of the microdischarges. At the edges of the microdischarges and in the interface, the current density was large enough that charging of the dielectric was complete, thereby removing nearly all the voltage from the gap which produced a less attaching environment. In those regions, the electron density has about the same density as the negative ions.

With a line voltage of 12 kV, the peak electron density is ten times larger than at 8.5 kV but, more importantly, the current density is large enough that the dielectric fully charges. This removes voltage from the gap which produces a less attaching environment, and results in a charged particle inventory which is dominantly electrons and positive ions. The final charged particle inventory is a sensitive func-

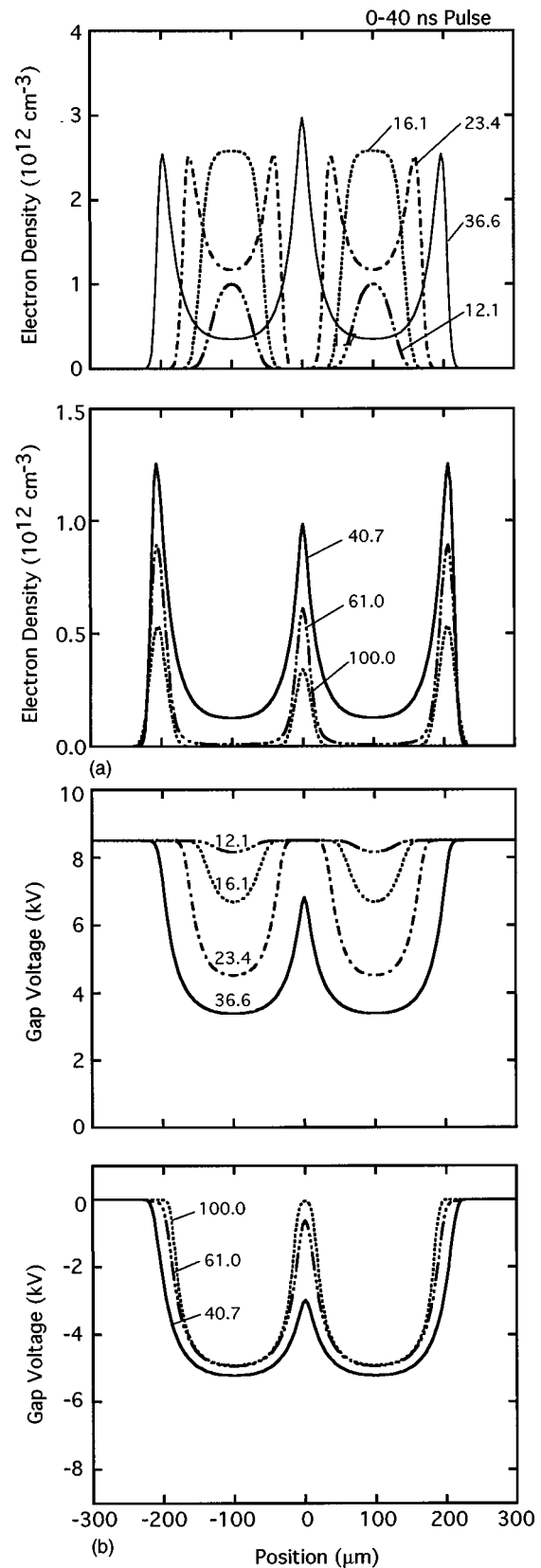


FIG. 7. Microdischarge properties along the axis of symmetry for $N_2/O_2=80/20$ microdischarges having a square wave 40 ns voltage pulse at 8.5 kV. (a) Electron density and (b) gap voltage. The curves are labeled with their time (ns) after the start of the voltage pulse. The separation of two microdischarges is $200 \mu m$. The residual E/N across the gap increases at attachment in the postavalanche phase, thereby consuming electrons.

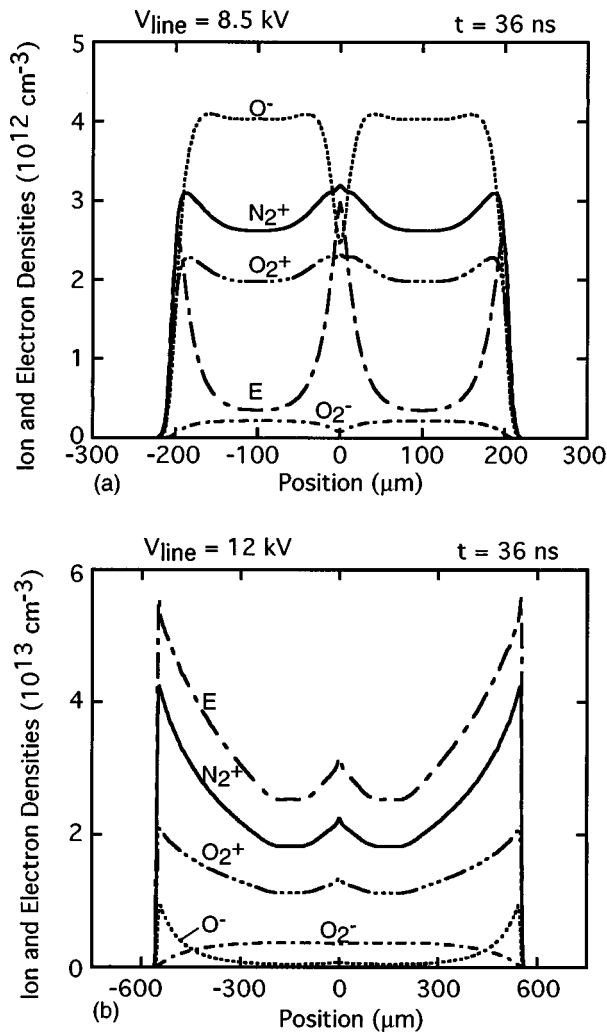


FIG. 8. Ion and electron densities for $N_2/O_2=80/20$ microdischarges at 36 ns for the conditions of Figs. 6 and 7. (a) An 8.5 kV and (b) 12 kV line voltage. O^- is the dominant negative charge carrier in the center of the microdischarge for lower line voltage while electrons are dominant for higher line voltages.

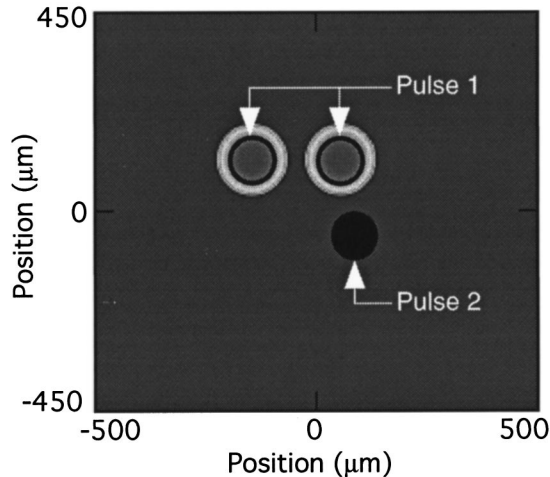


FIG. 9. Locations of microdischarges for Pulses 1 and 2, and residual charge on the dielectric resulting from Pulse 1 for a dry air microdischarge for the conditions of Fig. 7. The second pulse will have an inverse voltage from the first, and so the residual charge will add voltage to the applied potential.

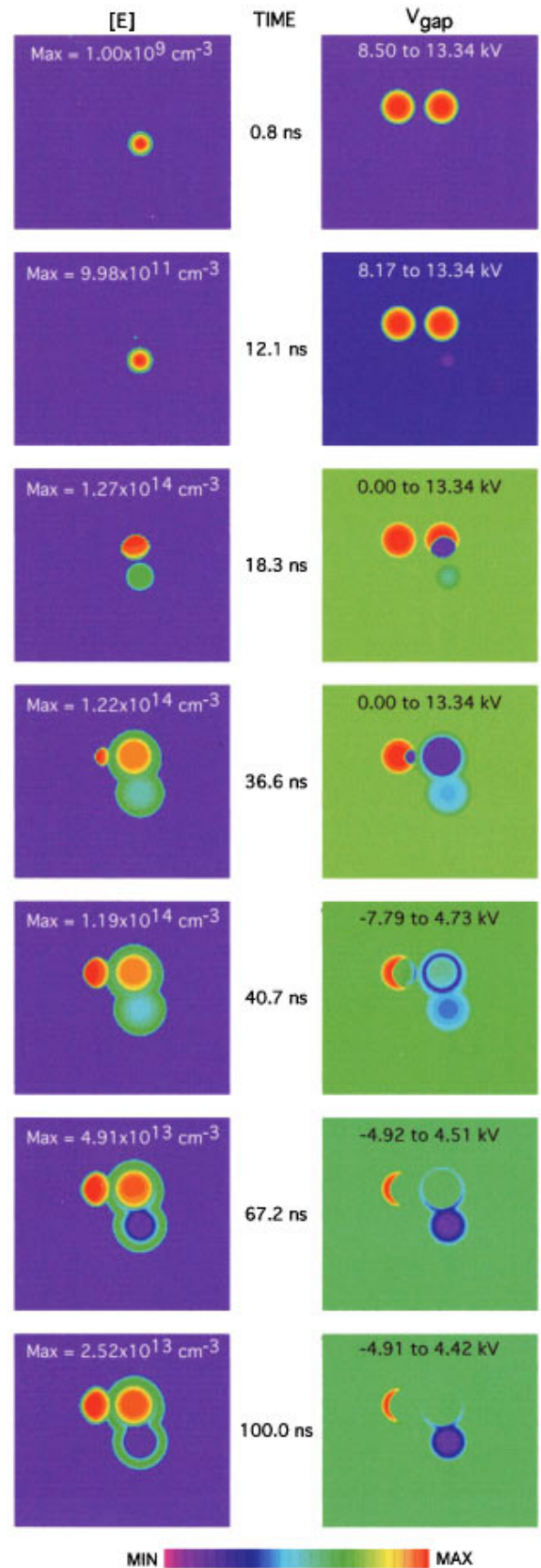


FIG. 10. Electron density and gap voltage at 0.8, 12.1, 18.3, 36.6, 40.7, 67.2, and 100.0 ns for the conditions of Fig. 9. The dynamic range of the color scale is 4 decades for the electron density. The daughter microdischarges avalanche to a higher density because of the larger E/N enabled by residual charge on the dielectric.

tion of the dependence of attachment on E/N in the sub-avalanche regime.

The residual charge on the dielectric from a previous discharge pulse can have a significant effect on the microdischarge dynamics of a subsequent pulse. To illustrate this dependence, we have set up the following conditions. A pair of microdischarges in dry air with a line voltage of 8.5 kV have previously occurred. Their locations, labeled "Pulse 1," are shown in Fig. 9. The voltage is sufficiently low that the dielectric is not fully discharged and there is residual charge left on the dielectric. On a second inverted voltage pulse, a single microdischarge, labeled "Pulse 2," occurs adjacent to the first pair. The residual charge left by the first pair of microdischarges then adds to the inverted line voltage on the second pulse. The resulting electron density and voltage across the gap during and after the second 40 ns voltage pulse are shown in Fig. 10 at 0.8, 12.1, 18.3, 36.6, 40.7, (just after the voltage pulse), 67.2, and 100.0 ns.

Initially (0.8 ns), the gap voltage is uniformly at 8.5 kV except where the residual voltage is left on the dielectric. At those locations the voltage is 13.3 kV. The electron density is initially large only in the vicinity of the second microdischarge. As the second microdischarge progresses (12.1 ns), it charges the dielectric beneath it thereby removing voltage from the gap. The electron density in the center of the microdischarge then decreases due to attachment. At the same time, the expanding microdischarge encroaches on the region of the dielectric which was previously charged. Since this region now has a larger gap voltage, electron avalanche rapidly occurs producing a "daughter" microdischarge (18.3 ns) having an even larger electron density than its "parent." The higher E/N for the first daughter microdischarge produces a higher current density which fully charges the dielectric, thereby removing voltage from the gap. The expansion of the first daughter microdischarge encroaches on the second high E/N region produced by the residual charge on the dielectric (36.6 ns). A second daughter microdischarge occurs, repeating the pattern of the first. The higher E/N produces a large current density which completely charges the underlying dielectric, thereby removing voltage from the gap. The electron densities in the center of the parent microdischarge are smaller than in the center of the daughter microdischarges due to the higher, but sub-avalanche, residual E/N in the center of the parent microdischarge.

At the end of the second pulse when the line voltage is pulled to zero, the second daughter microdischarge has yet to expand to fill the entire high E/N region (40.7 ns). A secondary avalanche occurs for both of the daughter microdischarges which fully discharges the dielectric in their domains (67.2 ns). The parent microdischarge, which was produced by the lower voltage which did not fully charge the dielectric, experiences a weak secondary avalanche which leaves residual charge on the dielectric. The end result (100 ns) is that residual charge (and voltage across the gap) is left on the

dielectric in the location of the parent microdischarge and in the peripheries of the daughter microdischarges.

IV. CONCLUDING REMARKS

A two-dimensional model has been developed to investigate microdischarge dynamics in dielectric barrier discharges operating in pure nitrogen and dry air. The electron density in a single microdischarge peaks in an expanding shell where the rate of avalanche is highest. In the interior of the microdischarge, where the dielectric is charged thereby removing voltage from the gap, the electron density is typically smaller due to the lower ionization rate and higher rates of electron loss processes at the lower E/N . The dynamics of adjacent expanding microdischarges which collide with each other are similar, with the exception that the electron density peaks at the interface by at most a few tens of percent. The expanding ionization waves of the individual microdischarges do not propagate through each other as would acoustic waves. The ionization waves are sustained by avalanche produced in regions of uncharged dielectric. Since the dielectric is charged by its partner in advance of the expanding microdischarge, the avalanche stalls at the interface. Residual charge on the dielectric from a previous microdischarge can significantly alter the dynamics of following microdischarges. The residual charge typically adds to the voltage for the subsequent microdischarge, thereby leading to more intense avalanche and providing a mechanism for microdischarges to expand beyond their single microdischarge domains.

ACKNOWLEDGMENTS

This work was supported by the National Science Foundation (CTS 94-12565, ECS 94-04133) and the Office of Naval Research (N00014-94-1-0819).

- ¹ *Non-Thermal Plasma Technique for Pollution Control*, edited by B. M. Penetrante and S. E. Schultheis (Springer, Berlin, 1993), Parts A and B.
- ² L. Bromberg, D. R. Chon, M. Koch, R. M. Patric, and P. Thomas, *Phys. Lett. A* **173**, 193 (1993).
- ³ B. M. Penetrante, M. C. Hsiao, B. T. Merritt, and G. E. Vogtlin, *Appl. Phys. Lett.* **66**, 3096 (1995).
- ⁴ W. Sun, B. Pashaie, S. K. Dhali, and F. I. Honea, *J. Appl. Phys.* **79**, 3438 (1996).
- ⁵ A. C. Gentile and M. J. Kushner, *J. Appl. Phys.* **79**, 3877 (1996).
- ⁶ A. Deryugin, A. Napartovich, C. Gorse, F. Paniccia, and M. Capitelli, *Plasma Chem. Plasma Process.* **17**, 79 (1997).
- ⁷ S. K. Dhali and I. Sardja, *J. Appl. Phys.* **69**, 6319 (1991).
- ⁸ M. C. Hsiao, B. T. Merritt, B. M. Penetrante, and G. E. Voglin, *J. Appl. Phys.* **78**, 3451 (1995).
- ⁹ R. G. Tonkyn, S. E. Barlow, and T. M. Orlando, *J. Appl. Phys.* **80**, 4877 (1996).
- ¹⁰ Z. Falkenstein, *J. Adv. Oxid. Technol.* **2**, 223 (1997).
- ¹¹ R. Morrow and J. J. Lowke, *J. Phys. D* **30**, 614 (1997).
- ¹² S. K. Dahli and D. F. Williams, *J. Appl. Phys.* **62**, 4696 (1987).
- ¹³ D. Braun, V. Gibalov, and G. Pietsch, *Plasma Sources Sci. Technol.* **1**, 166 (1992).
- ¹⁴ B. Eliasson and U. Kogelschatz, *IEEE Trans. Plasma Sci.* **19**, 309 (1991).
- ¹⁵ X. Xu and M. J. Kushner, *J. Appl. Phys.* **83**, 7522 (1998).